

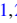





Formation and structure of $MuOH$ in ice studied by muon spin rotation

Amba Datt Pant ^{1,2,*}, Akihiro Koda ^{1,2}, Burkhard Geil,³ Katsuhiko Ishida ^{1,2}, Rajendra Adhikari ⁴, Kazuaki Kuwahata ⁵, Masanori Tachikawa,⁵ and Koichiro Shimomura ^{1,2}

¹*Institute of Materials Structure Science, High Energy Accelerator Research Organization, 1-1 Oho, Tsukuba, Ibaraki 305-0801, Japan*

²*Muon Section, Materials and Life Science Division, J-PARC center, 2-4 Shirane Shirakata, Tokai-mura, Naka-gun, Ibaraki 319-1195, Japan*

³*Institut für Physikalische Chemie, Universität Göttingen, Tammannstrasse 6, 37077 Göttingen, Germany*

⁴*Department of Physics, Kathmandu University, Dhulikhel, Kavre 45200, Nepal*

⁵*Graduate School of Nanobioscience, Yokohama City University, Yokohama, Japan*



(Received 19 April 2024; revised 22 August 2024; accepted 28 August 2024; published 11 September 2024)

The behavior of muons in water and ice is investigated by measuring spin rotation and relaxation of positive muons in water at 140–300 K, where we successfully observe oscillation in the zero-field spectra of muons in ice. The oscillation is attributed to the spin–dipole interactions between the muon in $MuOH$ and neighboring protons and to hyperfine transitions of triplet states of axially symmetric anisotropic muonium in ice. The Mu –H distance in $MuOH$ exceeds the H–H distance in H_2O by 5% in ice.

DOI: [10.1103/PhysRevB.110.104104](https://doi.org/10.1103/PhysRevB.110.104104)

Over the past four decades, muon spin rotation and relaxation (μ SR) measurements in water have been reported by several research groups [1–11]. A positive muon (henceforth referred to as muon) is similar to a proton with a lower mass ($m_\mu \sim 1/9m_p$, where m_μ and m_p are the masses of muon and proton, respectively). It is highly sensitive to magnetic fields in materials owing to its gyromagnetic ratio, which is 3.2 times that of a proton. In addition, two special features—100% spin polarization and asymmetric decay to positrons—make it an exotic probe for studying local electronic and spin dynamic states of materials. Its bound state with an electron is called muonium ($Mu = \mu^+e^-$), which is similar to a light isotope of an H atom with similar chemical behavior but with different magnetic properties. Both states, i.e., muon and muonium, reveal the microscopic information of materials via μ SR measurements.

Water in its liquid and solid states is a ubiquitous compound that plays important roles in many fields of modern science. The physics of water, its molecular structure and dynamics, and its complex phase behavior originate from the properties of its highly coordinated hydrogen-bond network, and these properties are guided by the Bernal–Fowler ice rules [12]. The well-known anomalies of liquid water—its large number of crystalline phases and polymorphism of its amorphous phases—make it a subject of great interest in condensed matter physics.

Muons injected into bulk water can serve as the most sensitive probes for the investigation of local structure and dynamics on subatomic length scales. Because a muon and muonium can substitute H^+ and H, respectively, they can be utilized as replacements for natural defects in ice. Zero-field (ZF) μ SR measurements reveal the magnetic environment at the muon stopping sites as well as the interaction between the

spins of muons and neighboring protons. Consequently, this technique extremely sensitive to the geometric arrangement of the closest neighboring protons. Using suitable model calculations, the local dynamics (rearrangements) can be analyzed within the average lifetime (2.2 μ s) of a muon at its stopping site.

Since the first observation of muonium formation in ice [1] and water [2], several μ SR studies have been conducted to investigate depolarization, missing fractions [5], and hyperfine interactions of muonium in water and ice [13]. When muons are injected into water, 60% of the injected muons exist in a diamagnetic form, 20% in the muonium form, and the remaining proportion is called the missing fraction. However, in ice, nearly 50% of the injected muon exists in a diamagnetic form, and the rest remains in the muonium form, with an almost negligible missing fraction. The missing fraction in water is attributed to the interaction of muonium with transient paramagnetic species, e.g., hydrated electrons, hydroxyl radicals, and hydrogen atoms (even to a small extent), formed by the radiolysis of water [6]. Hyperfine interactions and frequencies of muonium in water are induced by the anisotropy of the axial symmetry in the muonium hyperfine interaction. The magnitude of the splitting frequency of muonium depends on the angle between the applied field and crystal c axis of ice. Muonium shows spin-exchange interactions with molecular oxygen in water, and these interactions determine the relaxation rate of muonium in the presence of oxygen [11,14]. Level-crossing resonance measurements conducted by Cox *et al.* reveal that the muon is bound to O of H_2O and that there are two diamagnetic muon states ($HMuO$ and $H_2O-Mu^+-H_2O$) in ice [10,15,16]. However, measurements in HF-doped and NH_3 -doped ice could not confirm the formation site of $HMuO$ in Bjerrum L defects [17]. Similarly, Markland *et al.* reported the quantum diffusion of muonium in hexagonal ice (Ih) at low temperature of 8 K [18]. Most previously reported studies focused on muonium chemistry (or muonium

*Contact author: pant@post.kek.jp

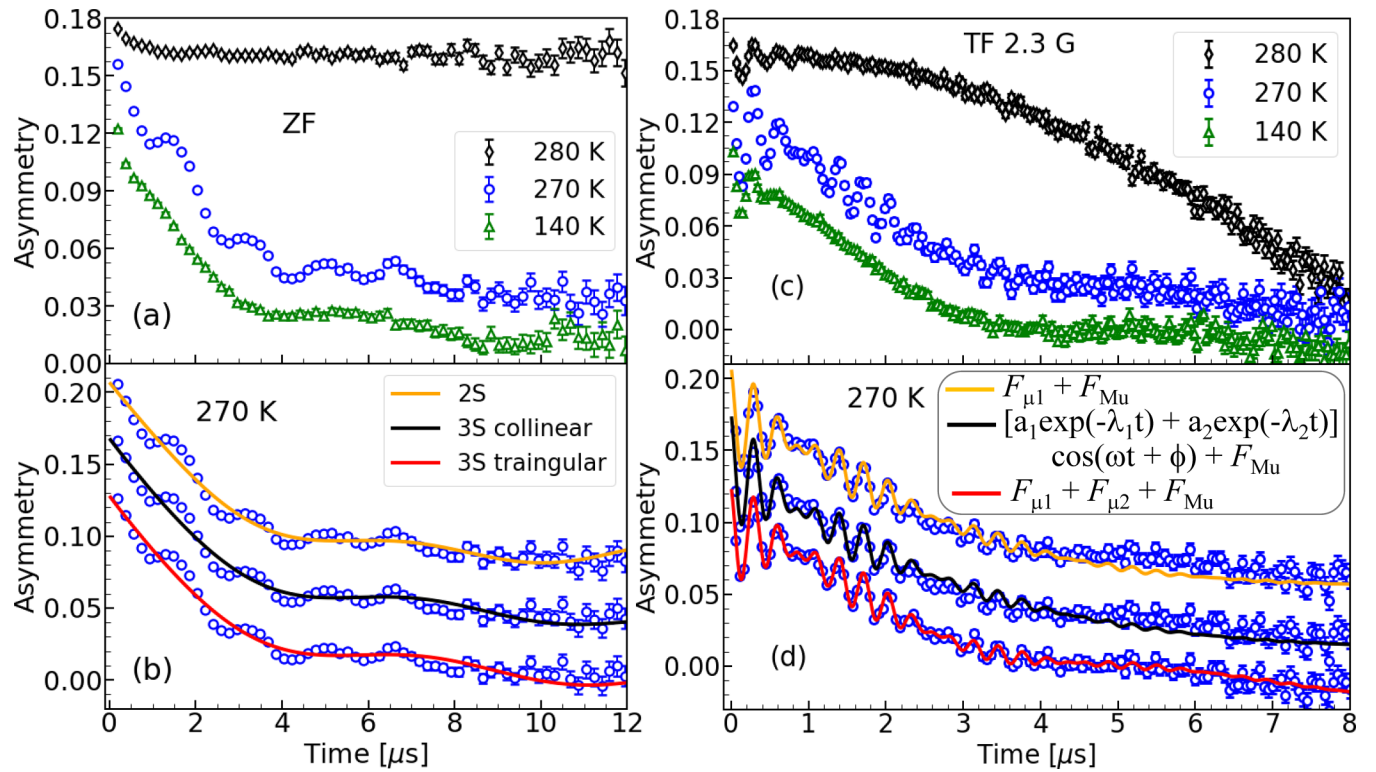


FIG. 1. (a) ZF μ SR time spectra of muons in water and ice; (b) fitting of the spectra at 270 K using polarization functions for 2S ($\chi^2 = 2.07$) [21], 3S collinear ($\chi^2 = 2.07$) [22], and 3S triangular ($\chi^2 = 2.08$) [23] systems; (c) TF 2.3 G μ SR time spectra of muons in water and ice; and (d) fitting of the TF 2.3 G spectra at 270 K using three fitting functions [$\chi^2 = 1.40$ (orange line), 1.55 (black), and 1.12 (red)]. The spectra are shifted for clarity.

behavior) in water and ice. However, the temperature-dependent behavior of muons in water remains obscure. Because the interactions of muons and muonium with materials are significantly different, investigations on the behavior of muons in water and ice are required to reinforce our understanding of the fundamental processes.

We performed μ SR experiments at S1 area in the S line of the Material and Life Science Facility at the Japan Proton Accelerator Research Complex (J-PARC) using 4-MeV spin-polarized muons. Water was collected from a Milli-Q (Advantage A10 system) water purification system, distilled twice, saturated with N_2 gas, and sealed (8.5 mL water) in an aluminum cell (volume 10 mL) under an N_2 environment. The aluminum cell was connected to a helium cryohead during the measurements. A muon beam (20-mm collimator) was injected into the water through an aluminum window (thickness = 0.1 mm; cross-sectional diameter = 43.5 mm). The cell was placed in a high-vacuum ($\sim 10^{-5}$ Pa) chamber connected to a flypast chamber. ZF and transverse-field (TF) measurements were carried out at different temperatures (140–300 K). In the ZF, the field value at the sample position was $\pm 1.0 \mu\text{T}$. The time histograms of the preferential decay of positrons from muons toward the muon spin directions were recorded using forward (N_F) and backward (N_B) detectors. The data were analyzed using the MUSRFIT software package [19]. The asymmetry parameter, defined by $A(t) = [N_F(t) - \alpha N_B(t)]/[N_F(t) + \alpha N_B(t)]$ (where α and t denote the balancing factor and time, respectively), was determined to evaluate the time evolution of the muon spin polarization.

Figure 1(a) depicts the time evolution of the positron decay asymmetry at the ZF at three selected temperatures. For $t > 1 \mu\text{s}$, a constant plateau is observed in the liquid state, while it disappears when the temperature is below the freezing point. In water, the initial relaxation ($t < 1 \mu\text{s}$) is induced by existing of the muonium fraction. At temperatures less than 270 K, the observed signal is a superposition of the relaxing decay curves with several oscillating contributions. Previously, Wang *et al.* [20] investigated the relaxing decay of muon polarization in various ice phases (ice II, ice VI, ice VIII, and high-density amorphous ice). However, they fitted a single exponential decay function to their ZF data and did not comment on superimposed oscillations.

In nonmagnetic materials, oscillations, similar to the ones observed in the ZF μ SR signal, are attributed to spin-dipole interactions between muons and nearby spin-one-half nuclei [21]. To date, several geometric arrangements of muons and nearby nuclei in two-spin (2S [21]) and three-spin systems (collinear [21,22], henceforth referred to as 3S collinear and equilateral triangular [23], henceforth 3S triangular) have been investigated [21–23]. However, Fig. 1(b) clearly demonstrates that the ZF μ SR data at 270 K cannot be interpreted using these models within the precision of the experimental data. At 270 K, two oscillating frequency components—one fast and another slow—are evident in the ZF spectra.

Figure 1(c) shows the TF 2.3 G μ SR spectra obtained at the three selected temperatures. The spectra obtained in liquid water displays distinct diamagnetic and paramagnetic muonium precession signals. By contrast, the spectra obtained

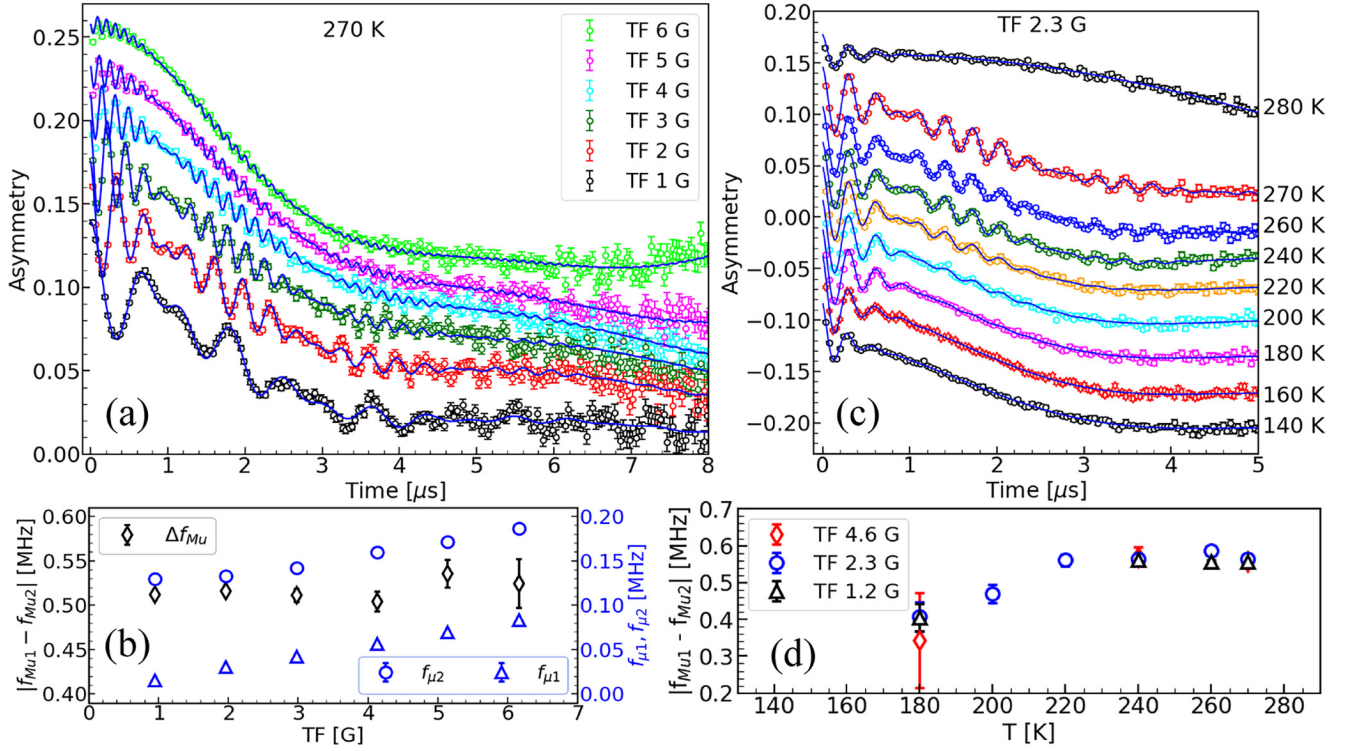


FIG. 2. (a) Fitting of the TF-dependent spectra obtained at 270 K; (b) splitting of muonium frequencies (Δf_{Mu} left vertical axis and frequencies of two diamagnetic muon species ($f_{\mu 1}$ and $f_{\mu 2}$ right vertical axis) under the TF field at 270 K; (c) temperature-dependent TF 2.3 G spectra; and (d) splitting of muonium frequencies with temperatures at three TF values. Time spectra in (a) and (c) are fitted using Eq. (1) and shifted for clarity.

in solid water (polycrystalline Ih) at 270 K exhibits a beating pattern of muonium frequencies in addition to the precession of the diamagnetic muon species. The beating pattern of muonium relaxes, i.e., disappears, below ~ 200 K. Unlike the spectra of single-crystal [7] and polycrystalline ice [6] reported by Percival *et al.*, the spectra obtained from ice in our study cannot be reproduced by a simple diamagnetic muon and the beating pattern of muonium [Fig. 1(d), orange line]. Moreover, the spectra obtained in the present paper cannot be reproduced by the functions used for two diamagnetic muon states detected in solutions of manganous nitrate hexahydrate in acetone and methanol [24] [Fig. 1(d), black line]. Here, to reproduce the TF spectra, we propose a function reflecting the field-dependent two diamagnetic muon species in addition to the beating pattern of muonium [Fig. 1(d) red line, and Eqs. (1)–(3)].

$$A_{TF}(t) = F_{\mu 1}(t) + F_{\mu 2}(t) + F_{Mu}(t), \quad (1)$$

$$F_{\mu i}(t) = A_{\mu i} \exp(-\lambda_{\mu i} t) \cos(\omega_{\mu i} t + \phi_{\mu i}), \quad (2)$$

$$F_{Mu}(t) = A_{Mu} \exp(-\lambda_{Mu} t) [\cos(\omega_{Mu} t + \phi_{Mu}) + \cos(\omega_{Mu} 2t + \phi_{Mu})], \quad (3)$$

where $\omega_i (= \gamma_i B_i = 2\pi f_i)$, A_i , ϕ_i , and λ_i are precession frequencies, amplitudes, initial phases, and relaxation rates of species i , respectively; γ_i is the gyromagnetic ratio of species i . To understand the temperature-dependent behavior of the oscillations in ZF and the presence of two diamagnetic muon species [$i = 1$ and 2 in Eq. (2)] in a TF, we performed

TF-dependent analysis in solid water [Figs. 2(a) and 2(b)], and temperature-dependent μ SR studies [Figs. 2(c) and 2(d)] at three TF values in ice. The spectra were analyzed using Eq. (1). Figure 2(b) (black open diamond) shows the splitting of the muonium frequencies; this splitting is almost field-independent under a weak field (< 10 G) at 270 K. This result reveals the occurrence of axially symmetric anisotropic hyperfine coupling (axially symmetric muonium hyperfine coupling tensors with $A_{xx} = A_{yy} \neq A_{zz}$ or full anisotropy with $A_{xx} \neq A_{yy} \neq A_{zz}$ [25]) of muonium in solid water. The splitting of muonium frequencies (Δf_{Mu}) is attributed to separation between two transitions (ν_{12} and ν_{23}) of anisotropic muonium triplet states [26]. Under the ZF, a single-frequency muonium oscillation is expected owing to the equal frequency of the ν_{12} and ν_{23} transitions (details in Appendix A)—this expected feature provides a crucial clue for analyzing ZF data [Fig. 1(a)]. The measured field-dependent precession frequencies of the two diamagnetic muon species (μ_1 and μ_2), presented in Fig. 2(b), indicate that the frequency of μ_2 is higher than that of μ_1 under the same TF field [$f_{\mu 1} = 0.015(1)$ MHz, $f_{\mu 2} = 0.130(2)$ MHz at TF 0.95 G]. Figure 2(d) displays the field- and temperature-independent muonium splitting, which is attributed to the axially symmetric anisotropic hyperfine coupling of muonium in ice and is consistent with previously reported data [7].

Based on the visualized hyperfine transitions of anisotropic muonium energy levels and field-dependent precession of the two diamagnetic muon species under a weak TF, the following generalized model [Eq. (4)] for analyzing the ZF spectra

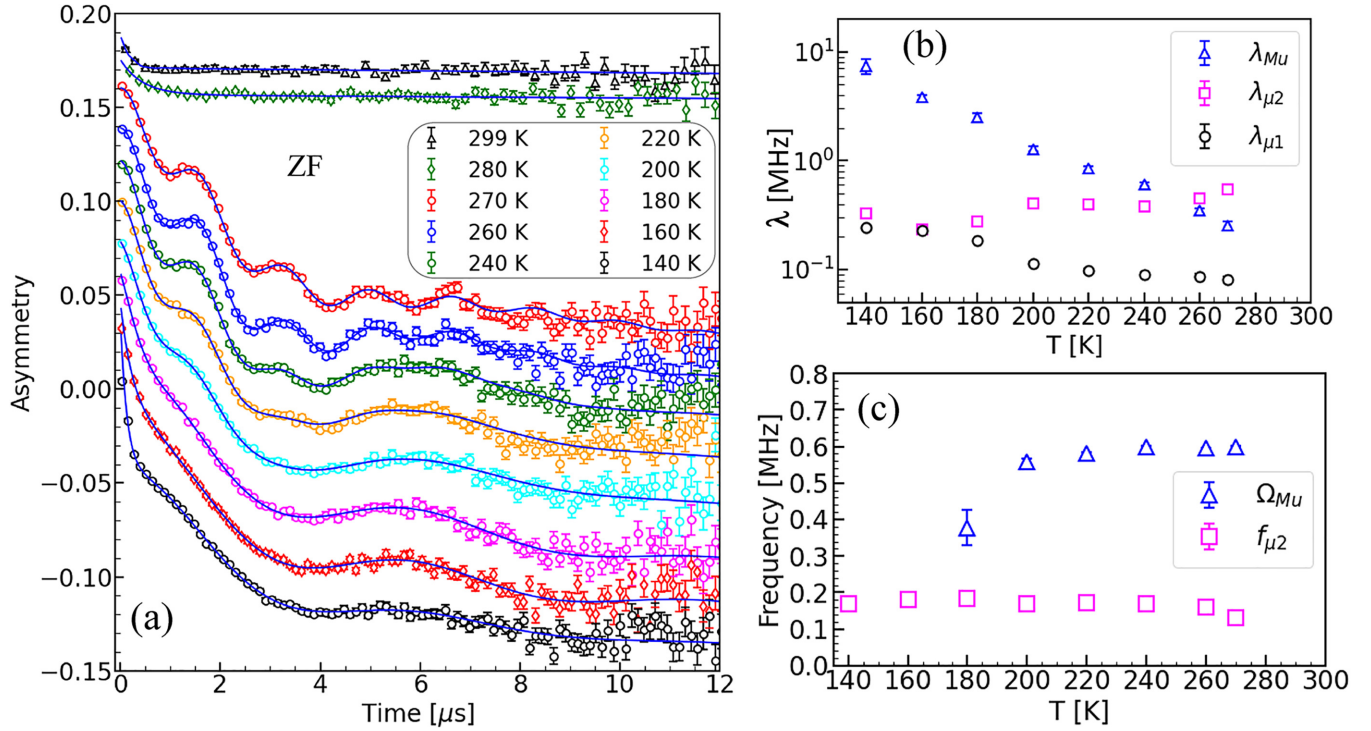


FIG. 3. (a) ZF μ SR spectra of water at different temperatures; the spectra obtained from solid water are fitted using Eq. (4) and shifted for clarity. (b) Relaxation rates of muonium and diamagnetic species with temperature. (c) Frequencies of anisotropic muonium and slow-oscillating signal (μ_2) under the ZF as function of temperature.

measured in solid water is proposed here:

$$\begin{aligned}
 A_{ZF}(t) = & A_{Mu} \exp(-\lambda_{Mu}t) \left[\frac{1}{6} + \frac{1}{3} \cos(\Omega_{Mu}t) \right] \\
 & + A_{\mu_2} \exp(-\lambda_{\mu_2}t) \cos(\omega_{\mu_2}t + \phi_{\mu}) \\
 & + A_{\mu_1} \exp(-\lambda_{\mu_1}t),
 \end{aligned} \quad (4)$$

where the first term corresponds to the powder average of the polarization function of anisotropic muonium under the ZF, neglecting the terms containing transitions between singlet ground and triplet excited states [27]; the second and third terms correspond to the diamagnetic muon species μ_2 and μ_1 , respectively; Ω_{Mu} represents the oscillating frequency of anisotropic muonium corresponding to the ν_{23} transition under the ZF. The fitted ZF spectra and corresponding parameters are presented in Figs. 3(a), 3(b) and 3(c), respectively. The determined dipole anisotropy ($\omega_{dip} = 2\Omega_{Mu}$) of the hyperfine interaction of muonium at 270 K is 1.2034(38) MHz. Figure 3(b) shows that the relaxation rate of muonium increases with decreasing temperatures. In Fig. 3(c), the slow-oscillating signal (f_{μ_2}) appears to remain constant over the measured temperature range; however, the fast-oscillating signal (Ω_{Mu}) originating from the axially symmetric anisotropic hyperfine coupling of muonium becomes invisible below 180 K because of the high relaxation rate of muonium. The nuclear dipolar coupling of protons with muonium increases the relaxation rate, thereby preventing the detection of muonium oscillations below 180 K.

Next, we focus on identifying these two diamagnetic muon species in solid water. First, following the mechanism of proton transfer in ice, we consider that some of the injected

muons can replace one of the protons of water and form $MuOH$. A quantum simulation (details in Appendix B), performed by considering the spin-dipole interactions between a muon and neighboring protons (here, we consider a muon and three nearby protons, i.e., in total a four spin-one-half system, 4S), shows that the frequency, which depends on the distance between the muon and protons, is less than 0.2 MHz. This frequency value is comparable with the low frequency of the oscillating signal detected under ZF [Fig. 3(c), open square] and that of μ_2 under the weak TF [Fig. 2(b) open circle]. Therefore, the slow-oscillating diamagnetic muon (μ_2) signal detected in solid water is attributed to $MuOH$. By replacing the term $\cos(\omega_{\mu_2}t + \phi_{\mu})$ in Eq. (4) by the polarization function of $MuOH$ in the 4S system, $G_{MuOH}(t)$, the ZF spectra recorded at 270 K can be well reproduced [Fig. 4(a)] when the $Mu-H$ distance (1.65 Å) in $MuOH$ exceeds the H-H distance in H_2O by 5% (details in Appendix B). The long $Mu-H$ distance in $MuOH$ can be achieved either via elongation of the $Mu-O$ bond or reorientation of the water molecule. Our path integral simulation results of $MuOH$ in Ih at 250 K shows 9% elongation of the $Mu-O$ bond and a <1% angle (details in Appendix C). The experimental data (microsecond range) may reflect the bond elongation rather than the fast reorientation (\sim picosecond) of the water molecule. Based on the initial asymmetries of each term, the determined fractions of μ_1 , $MuOH$, and muonium at 270 K are 29.0(5)%, 33.7(4)%, and 17.5(6)%, respectively, with the remaining representing the missing fraction (temperature-dependent fractional yield explained in Appendix D). In the first and second terms of Eq. (4), the exponential decay components account for the

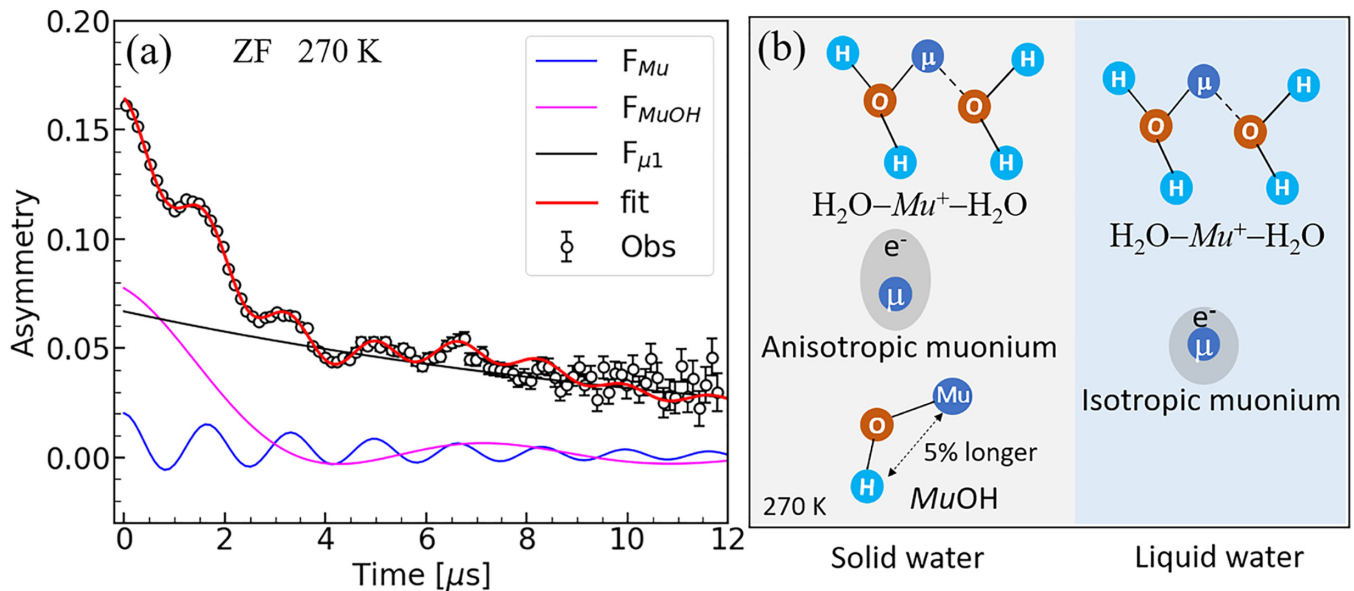


FIG. 4. (a) Fitting of the ZF spectra (α corrected), recorded at 270 K using the polarization function of $MuOH$ in addition to those of a diamagnetic muon (μ_1 , which may be $H_2O-Mu^+-H_2O$) and anisotropic muonium contribution. The fast-oscillating signal is attributed to the axially symmetric anisotropic hyperfine coupling of muonium, whereas the slow-oscillating signal is attributed to the spin-dipole interaction of the muon in $MuOH$, where $F_{MuOH}(t) = A_{\mu_2} \exp(-\lambda_{\mu_2} t) G_{MuOH}(t)$. (b) Schematic of the muon species in liquid water at 280 K and solid water at 270 K. In the case of solid water, the time spectra corresponding to three muon species ($H_2O-Mu^+-H_2O$, $MuOH$ and anisotropic muonium) are observed.

polarization decoherence due to the higher-order terms in the interaction between the muon and next-neighbor nuclear spins. Even though the exponential term is purely phenomenological, the relaxing oscillation is evident. The oscillating ZF spectra exhibited by fluoride crystals (CaF_2 and NaF) [28] have been successfully explained, including the interaction between muons and more distant nuclear spins. However, in ice, the implanted muons can create defects, and subsequently, the Bjerrum defect dynamics may cause reorientation of the water molecules [29]. For such a dynamic system, derivation of the polarization function considering the effect of nearby and more distant protons around the muon sites is computationally costly.

Among the two diamagnetic muon species (μ_1, μ_2) mentioned above, μ_2 is attributed to $MuOH$ and μ_1 to $H_2O-Mu^+-H_2O$ as pointed out from the LCR study by Cox *et al.* [10,16,17]. Their LCR measurement in ice doped with HF and NH_3 pointed out the existence of both $MuOH$ and $H_2O-Mu^+-H_2O$. In conventional μSR (weak TF and ZF) we observed the distinct frequencies in the time spectra corresponding to both diamagnetic muon species in ice for the first time. The revised model of Leung *et al.* [30] indicates the formation of the diamagnetic MuH molecule in liquid water. However, no noticeable signal of MuH was observed in the liquid and solid water spectra measured under our experimental conditions (details in Appendix E).

Due to the fast motion of the hydrogen bonding networks [31] in liquid water, the $MuOH$ signal is averaged out and cannot be detected. Therefore, signals of only two states of muon, i.e., a diamagnetic muon and paramagnetic isotropic muonium, are detected in the spectra measured in liquid water [Fig. 4(b)]. By contrast, in the spectra recorded in solid water,

because of the stable configuration of $MuOH$ in μs time range, we found a distinct signal corresponding to $MuOH$ with long $Mu-H$ distance in addition to another diamagnetic muon state ($H_2O-Mu^+-H_2O$) and an anisotropic muonium.

Our paper provides a powerful tool for investigating the defect-mediated proton dynamics in various phases of hydrogen-bonded ice. The muon implanted in the ice crystal creates—and is a part of these—defects (Bjerrum L and D defects) that induce translational and rotational proton or H_2O molecule dynamics in solid-ice phases. The findings of this paper may provide insights into the spin dynamics observed in other systems, e.g., proton dynamics in hydrated organic materials, proton transfer in biological membranes, and general transport processes of other spin-nuclei in solid state materials.

In conclusion, the oscillations detected in the ZF time spectra obtained from solid water are attributed to the spin-dipole interactions between the muon in $MuOH$ and nearby protons as well as the hyperfine transitions of the triplet states of axially symmetric anisotropic muonium in ice. Our detailed analysis of muon spin rotation under a ZF and weak TF correlates the distinct time spectra with $MuOH$, providing direct evidence of molecular $MuOH$ formation in ice. The $Mu-H$ distance in $MuOH$ exceeds the $H-H$ distance in H_2O by 5% in ice.

A.D.P. thanks J. Lord, F. Pratt, K. Nagamine, J. Sugiyama, R. Kadono, K. Fukutani, P. C. Gupta, M. Hiraishi, S. Nishimura, T. U. Ito, S. Kanda, I. Umegaki, and J. Nakamura for their help and discussions. The muon experiments were performed at the Materials and Life Science Experimental Facility of the J-PARC under a user program

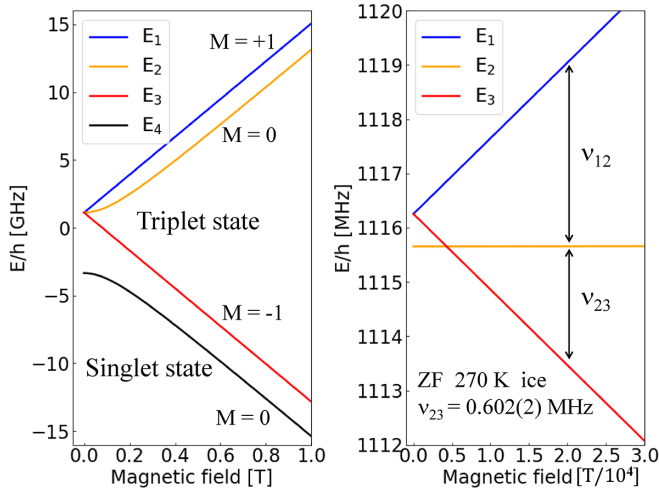


FIG. 5. Breit-Rabi diagram for anisotropic muonium in ice. Left: Singlet ground and excited triplet states. Right: Zoomed image of the left figure, showing the hyperfine transitions of the triplet state under a TF of 0.3 mT. Two frequencies (ν_{12} and ν_{23}) of muonium with a splitting frequency of ($\nu_{12} - \nu_{23}$) are observed under a weak field. Under the ZF, the single frequency ($\nu_{23} = 0.602(2)$ MHz) oscillating signal is observed at 270 K in the case of solid water owing to the axially symmetric anisotropic hyperfine coupling of muonium.

(Proposals No. 2019B0412, No. 2020A0298, No. 2021B0332, No. 2022A0264, and No. 2023A0198). This work is supported by a Grant-in-Aid for Scientific Research of the Ministry of Education, Culture, Sports, Science and Technology (MEXT), JSPS, KAKENHI (Grant No. 21K15583).

APPENDIX A: HYPERFINE TRANSITIONS OF ANISOTROPIC MUONIUM

Muonium is a bound state of two spin-one-half particles: a muon and an electron. The total Hamiltonian of an anisotropic muonium in an external TF (\mathbf{B}_{ext}) applied along the z axis is given by [27]

$$H = \hbar \mathbf{S}_e \mathbf{A} \mathbf{S}_\mu + g_e \mu_B B_{\text{ext}} S_e^Z - \hbar \gamma_\mu B_{\text{ext}} S_\mu^Z, \quad (\text{A1})$$

where \mathbf{A} is the anisotropic hyperfine coupling tensor. Upon solving the Hamiltonian, the determined variations in the four energy eigenvalues (E_1 , E_2 , E_3 , and E_4) with the external field strength are illustrated using the Breit-Rabi diagram (Fig. 5). If up and down spins are denoted by $|1/2\rangle$ and $|-1/2\rangle$, respectively, then the corresponding four basis states $|m_e, m_\mu\rangle$ are $|1/2, 1/2\rangle$, $|1/2, -1/2\rangle$, $|-1/2, 1/2\rangle$, and $|-1/2, -1/2\rangle$. The eigenvectors of the muonium states corresponding to the eigenvalues are given by $|\psi_1\rangle = |1/2, 1/2\rangle$, $|\psi_2\rangle = c_1|1/2, -1/2\rangle + c_2|-1/2, 1/2\rangle$, $|\psi_3\rangle = |-1/2, -1/2\rangle$, and $|\psi_4\rangle = c_1|1/2, -1/2\rangle - c_2|-1/2, 1/2\rangle$. This result shows that levels 1 and 3 are pure states, whereas, levels 2 and 4 are coherent mixtures of the $|1/2, -1/2\rangle$ and $|-1/2, 1/2\rangle$ states. A detailed explanation is available elsewhere [27]. Figure 5 (left) depicts the single ground state and excited triplet states of anisotropic muonium in solid water. Under a weak TF [Fig. 5 (right)], the two frequencies of muonium observed in ice correspond to ν_{12} and ν_{23} , and

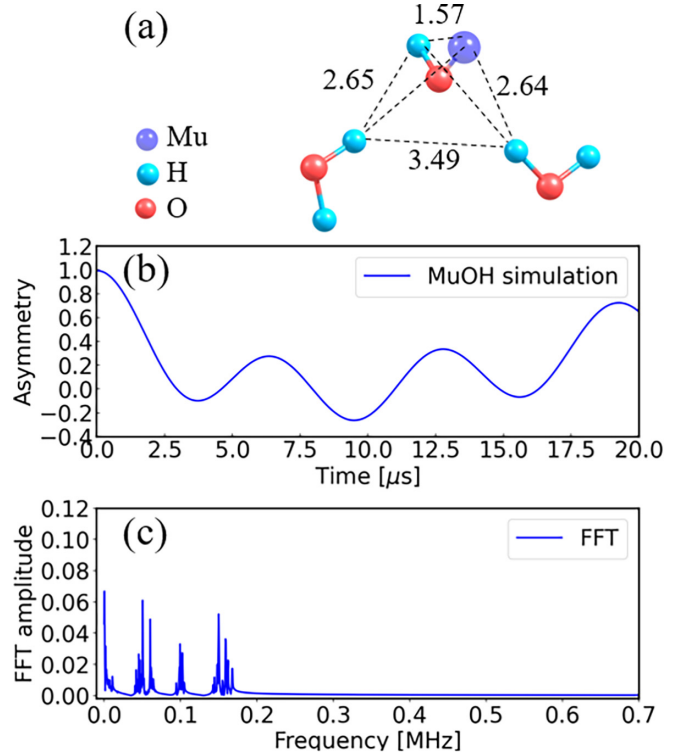


FIG. 6. (a) Schematic of $MuOH$, which forms when a muon replaces one of the protons in the Ih structure with two nearby H_2O . The dotted lines show the distances of the muon and protons in Å. We consider spin-dipole interactions between a muon and three nearby protons, which collectively form a 4S system. (b) Polarization function $G_{MuOH}(t)$ and (c) its FFT. The maximum frequency of the signal is less than 0.2 MHz, which is comparable to the frequencies of low-frequency and μ_2 signals observed under ZF and weak TF, respectively.

the splitting frequency of muonium is equivalent to their difference ($\nu_{12} - \nu_{23}$) [26]. Under the ZF, the observed single-frequency muonium is ascribed to the equal transitions frequencies ($\nu_{12} = \nu_{23}$). At 270 K under ZF, we obtain $\nu_{23} = 0.602(2)$ MHz in ice [(Fig. 5 (right))]. Visualizing the splitting between the singlet ground and triplet states through conventional muon measurements is challenging.

APPENDIX B: QUANTUM SIMULATION BASED DERIVATION OF POLARIZATION FUNCTION

The $MuOH$ forms when a muon replaces one of the protons in H_2O . The spin Hamiltonian of $MuOH$, considering the four spin-half systems [a muon and three protons of surrounding water molecules, Fig. 6(a)], can be expressed as

$$H = \sum_{i>j}^4 \frac{\gamma_i \gamma_j}{\mu_0 r_{ij}^3} (3S_i \cdot S_j - (S_i \cdot r_{ij})(S_j \cdot r_{ij})), \quad (\text{B1})$$

where $i, j = 1, 2, 3, 4$ correspond to three protons and a muon; r_{ij} is the vector joining the spins S_i and S_j ; γ_i and γ_j are the gyromagnetic ratios of the spin-half particles, respectively.

For the quantum simulation, the Quantum code [32] was used to solve the time evolution of the muon spin using the density matrix method. The spin evolution of muon, due to

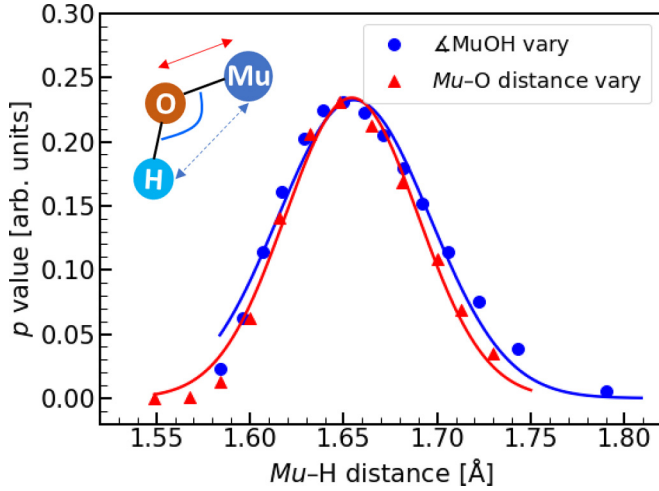


FIG. 7. χ^2 distribution (p value) versus $Mu-H$ distance in $MuOH$ for the ZF data, obtained at 270 K, fitted using Eq. (B3). The blue (blue line is fit) and red marks, corresponding to $Mu-H$ distance, are obtained by changing the $MuOH$ angle and $Mu-O$ bond length, respectively.

its dipole interactions with the three nearby protons (total four spin-one-half system, 4S), was estimated by solving the Hamiltonian matrix of order ($2^4 \times 2^4$). The powder averaged polarization function for the simple model under the ZF was developed in the form of Eq. (B2) as shown below:

$$G_{MuOH}(t) = \sum_k^{256} C_k \cos(\omega_k t) + D_k \sin(\omega_k t), \quad (B2)$$

where $k = 1, 256$ is attributed to the solution of the spin-Hamiltonian matrix of order $2^4 \times 2^4$ associated with the 4S system; C_k and D_k are the coefficients of the real and imaginary terms of the polarization functions for the 4S system. The coefficients (i.e., D_k) of the imaginary terms vanish.

Figure 6(a) shows schematic of a muon in the 4S system, and its polarization function [$G_{MuOH}(t)$] and the corresponding FFT result are presented in Figs. 6(b) and 6(c), respectively. The frequency range of the spectra is up to 0.167 MHz, which is comparable to the frequencies of the low-frequency and μ_2 signals observed under the ZF and weak TF, respectively.

The ZF spectra obtained at 270 K were analyzed for different geometries (changing bond length or bond angle) of $MuOH$ by varying the $Mu-H$ distance in $MuOH$ and by using the following fitting equation, Eq. (B3):

$$\begin{aligned} A_{ZF}(t) = & A_{Mu} \exp(-\lambda_{Mu}t) \left[\frac{1}{6} + \frac{1}{3} \cos(\Omega_{Mu}t) \right] \\ & + A_{\mu_2} \exp(-\lambda_{\mu_2}t) G_{MuOH}(t) \\ & + A_{\mu_1} \exp(-\lambda_{\mu_1}t). \end{aligned} \quad (B3)$$

The Gaussian fit of the probability density function (χ^2 distribution; p value [33]) of both cases, i.e., (a) varying $Mu-H$ by changing the $MuOH$ angle (blue line and marker in Fig. 7) and (b) varying $Mu-H$ distance by changing $Mu-O$

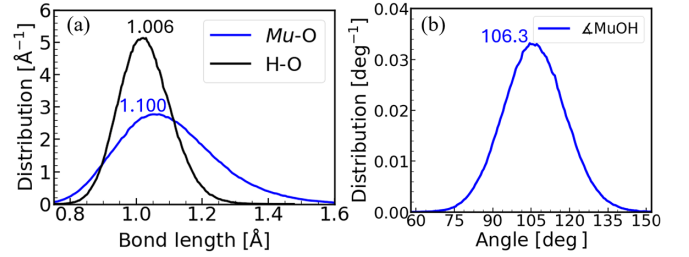


FIG. 8. PIMD simulation results at 250 K: (a) Distribution of $Mu-O$ and $H-O$ bonds and (b) angle of $MuOH$ in solid water.

bond length (red lines and markers in Fig. 7), shows that the peak values correspond to 1.656(1) Å and 1.654(1) Å, respectively. This shows that the $Mu-H$ distance in $MuOH$ exceeds the $H-H$ distance in H_2O by 5% in ice.

APPENDIX C: PATH INTEGRAL MOLECULAR DYNAMIC SIMULATIONS FOR $MuOH$ IN ICE

We performed the path integral molecular dynamics (PIMD) simulations to understand the $MuOH$ geometry in ice. The mass of the muon (i.e., Mu in $MuOH$) is approximately one-ninth that of a proton, and the quantum effect of Mu is significant for theoretical simulations of Mu . The PIMD simulation includes the full-dimensional quantum effect of Mu , which is based on the Feynman path integral formulation. In the simulation, the bead expansion of the ring polymer was used to account for the quantum effects of the nucleus (muon). The PIMD simulations were performed by modifying an existing house code [34,35]. For the sampling of the simulations, the temperatures were set to 250 K, with Nosé-Hoover chain thermostats introduced to achieve a canonical (NVT) ensemble. The total sampling steps for the simulations were 50 000. The time-step size for the simulations with muon and without muon were 0.04 and 0.1 fs, respectively. The interatomic potentials were obtained using the VASP package [36,37] with pseudopotentials derived using the projector augmented plane wave method. The Perdew-Burke-Ernzerho functional was utilized, along with a cutoff energy of 500 eV, and the Brillouin zone of sampling was restricted to the Γ point for density functional calculations. Mu injected into the ice was modeled as 12 water molecules (one $MuOH$ and 11 H_2O molecules) with periodic boundary conditions. The lattice constants were optimized using the VASP package prior to performing the PIMD simulations.

The bond lengths ($H-O$, $Mu-O$) and bond angle (of $\angle MuOH$) obtained from PIMD simulations are shown in Figs. 8(a) and 8(b), respectively. The quantum effect of muon significantly increases the bond length. The expectation values of bond lengths of $Mu-O$ and $H-O$ are 1.100 and 1.006 Å, respectively, at 250 K [Fig. 8(a)]. The expectation value of the bond angle (of $\angle MuOH$) is 106.3 deg [Fig. 8(b)]. These results indicate that the $Mu-O$ bond in $MuOH$ shows 9% elongation due to vibrational motion. Elongation of the $Mu-C$ bond, with respect to the $H-C$ bond after cleaving of the double bond and formation of muoniated radicals, has been reported in unsaturated organic

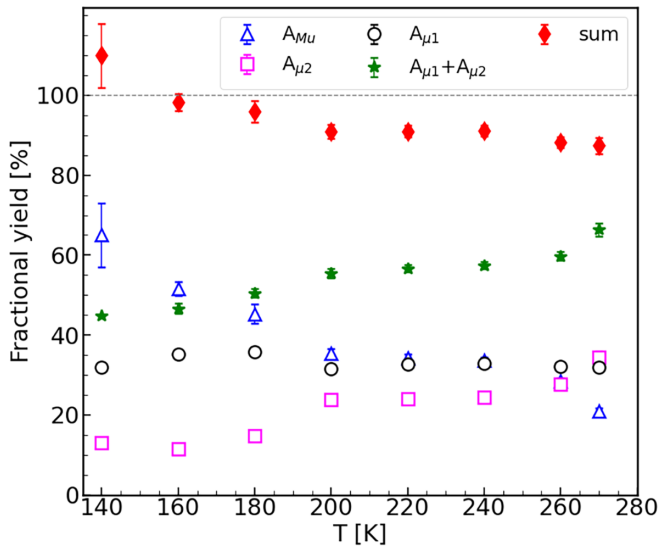


FIG. 9. Variation in the initial asymmetries of each muon species, i.e., μ_1 , μ_2 , and anisotropic muonium, with temperature, derived from the ZF time spectra. The dotted line corresponds to the full asymmetry in the spectrometer for silver.

molecules like cyclohexadienyl, cyclopententyl [38], butene [39], and ethylene [40].

APPENDIX D: TEMPERATURE-DEPENDENT FRACTIONAL YIELD DERIVED FROM OSCILLATING ZF SPECTRA

Figure 9 presents the asymmetries of each muon species, i.e., two diamagnetic muons (μ_1 and μ_2) and an anisotropic muonium, derived by analyzing the temperature-dependent oscillating ZF spectra using our proposed model [Eq. (4)]. The dotted line corresponds to the full asymmetry (0.24) observed in the spectrometer for a blank sample (silver). At low temperature (<200 K), the high relaxation rate of muonium indicates the increasing asymmetry of muonium. The total diamagnetic muon fraction (green star) decreases with decreasing temperature, showing consistency with previously reported data obtained from TF measurements [6,10]. The missing fraction, which is due to the interaction of radiolysis products with muonium [6] in ice at an early time (nanosecond order), is detected at temperatures above 160 K; this temperature is consistent with the results of a previous study, in which a missing fraction has been observed in single-crystal ice at >200 K, but not in polycrystalline ice [7]. Although previous reports indicate that the total diamagnetic muon fraction in ice varies with temperature, our results reveal the temperature dependence of the $MuOH$ fraction.

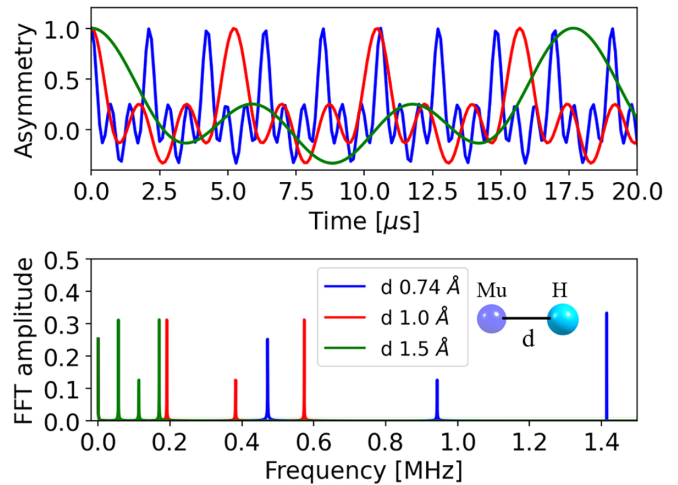


FIG. 10. Simulation of MuH at three selected $Mu-H$ distances ($d = 0.74, 1.0$ and 1.5 Å). Time spectra (upper panel) and the corresponding FFT results (lower panel).

APPENDIX E: QUANTUM SIMULATION OF THE MuH MOLECULE

The spin-dipole interaction between a muon and proton in MuH was calculated using Eqs. (B1) and (B2) for two a spin-half system. Figure 10 depicts the derived polarization function and the corresponding FFT at three selected distances. The estimated maximum frequencies of the MuH system for the $Mu-H$ distances of 0.74 Å (similar to H-H), 1.0 , and 1.5 Å are 1.42 , 0.56 , and 0.17 MHz, respectively. If the $Mu-H$ distance is similar to the H-H distance, then a signal at 1.42 MHz should be detected in the corresponding weak TF and ZF spectra. However, no such frequency signal was observed at the present precision of the μSR time spectra. If the $Mu-H$ distance in ice is 1.0 Å, then a 0.56 MHz signal with a field-dependent behavior should be visible in the weak TF scans. In contrast, the weak TF spectra exhibited an almost field-independent frequency that was assigned to the hyperfine transitions of anisotropic muonium. A muon, at a distance of 1.5 Å from a proton, can produce such a low-frequency signal (<0.2 MHz) under a ZF and weak TF; notably, this distance is almost the same as that between a muon and proton in a $MuOH$ molecule [Fig. 6(a)] and is not that expected for an isolate MuH molecule.

The TF spectra obtained in liquid water can be well reproduced by accounting for the Larmor precession of a diamagnetic muon and another paramagnetic muonium. This result indicates that within a microsecond timescale, distinct time spectra of the $MuOH$ and MuH molecules are not detected in liquid water. The averaged-out $MuOH$ signal in the microsecond timescale can be attributed to the rapidly changing of hydrogen-bond networks and fast dynamics of water molecules ($MuOH$) in liquid water.

- [1] G. Myasishcheva, Y. V. Obukhov, V. Roganov, and V. Firsov, A search for atomic muonium in chemically inert substances, *Sov. Phys. JETP* **26**, 298 (1968).
- [2] P. W. Percival, H. Fischer, M. Camani, F. N. Gyax, W. Rüegg, A. Schenck, H. Schilling, and H. Graf, The detection of muonium in water, *Chem. Phys. Lett.* **39**, 333 (1976).
- [3] K. Nagamine, K. Nishiyama, J. Imazato, H. Nakayama, M. Yoshida, Y. Sakai, H. Sato, and T. Tominaga, Long-lived muonium in water revealed by pulsed muons, *Chem. Phys. Lett.* **87**, 186 (1982).
- [4] P. W. Percival, J. C. Brodovitch, S. K. Leung, and K. E. Newman, Muonium in ice, *Hyperfine Interact.* **18**, 543 (1984).
- [5] P. W. Percival, The missing fraction in water, *Hyperfine Interact.* **8**, 325 (1981).
- [6] P. W. Percival, E. Roduner, and H. Fischer, Radiolysis effects in muonium chemistry, *Chem. Phys.* **32**, 353 (1978).
- [7] P. W. Percival, K. M. Adamson-Sharpe, J. C. Brodovitch, S. K. Leung, and K. E. Newman, Partial spin depolarization of muonium in ice, *Chem. Phys.* **95**, 321 (1985).
- [8] M. Camani, F. N. Gyax, W. Rüegg, A. Schenck, H. Schilling, H. Graf, W. Kündig, B. D. Patterson, P. Roggwiller, H. Fischer, and P. W. Percival, Muon spin rotation studies at SIN, *Hyperfine Interact.* **2**, 83 (1976).
- [9] D. C. Walker, Y. C. Jean, and D. G. Fleming, Muonium atoms and intraspur processes in water, *J. Chem. Phys.* **70**, 4534 (1979).
- [10] S. Cox, J. Smith, and M. Symons, Measurement of ^{17}O quadrupole interactions and identification of the diamagnetic fraction in ice by muon level crossing resonance, *Hyperfine Interact.* **65**, 993 (1991).
- [11] E. Roduner, P. L. W. Tregenna-Piggott, H. Dilger, K. Ehrensberger, and M. Senba, Effect of mass on particle diffusion in liquids studied by electron spin exchange and chemical reaction of muonium with oxygen in aqueous solution, *J. Chem. Soc., Faraday Trans.* **91**, 1935 (1995).
- [12] J. D. Bernal and R. H. Fowler, A theory of water and ionic solution, with particular reference to hydrogen and hydroxyl ions, *J. Chem. Phys.* **1**, 515 (1933).
- [13] E. Roduner, P. W. Percival, P. Han, and D. M. Bartels, Isotope and temperature effects on the hyperfine interaction of atomic hydrogen in liquid water and in ice, *J. Chem. Phys.* **102**, 5989 (1995).
- [14] A. D. Pant, K. Nagamine, E. Torikai, I. Shiraki, K. Shimomura, F. L. Pratt, H. Ariga-Miwa, K. Ishida, and J. S. Schultz, Muonium response to low oxygen levels in haemoglobin and other biological aqueous solutions and potential application towards monitoring hypoxia, *Nucl. Instrum. Methods Phys. Res. Sect. A* **1011**, 165561 (2021).
- [15] S. Cox, G. Eaton, J. Magraw, and C. Scott, Muon addition to oxygen in ice: Characterisation of the diamagnetic product by level crossing resonance, *Chem. Phys. Lett.* **160**, 85 (1989).
- [16] S. Cox, μSR studies of ice, illustrating the positive muon as a magnetic resonance probe of structure and dynamics, *Phys. Scr.* **1992**, 292 (1992).
- [17] S. Cox, N. A. De Campos, P. Mendes, J. Gil, A. Kratzer, V. Nield, and J. Smith, Level crossing resonance in ice: Identification of two diamagnetic muon states, *Hyperfine Interact.* **86**, 747 (1994).
- [18] T. E. Markland, S. Habershon, and D. E. Manolopoulos, Quantum diffusion of hydrogen and muonium atoms in liquid water and hexagonal ice, *J. Chem. Phys.* **128**, 194506 (2008).
- [19] A. Suter and B. Wojek, Musrfit: A free platform-independent framework for μSR data analysis, *Phys. Procedia* **30**, 69 (2012).
- [20] Y. Wang, S. Dong, A. Kolesnikov, P. Zhang, and J. Li, Muon-spin-relaxation studies of high pressure phases of ices, *Physica B: Condens. Matter* **350**, E451 (2004).
- [21] J. H. Brewer, S. R. Kreitzman, D. R. Noakes, E. J. Ansaldo, D. R. Harshman, and R. Keitel, Observation of muon-fluorine “hydrogen bonding” in ionic crystals, *Phys. Rev. B* **33**, 7813 (1986).
- [22] R. Kadono, K. Shimomura, K. H. Satoh, S. Takeshita, A. Koda, K. Nishiyama, E. Akiba, R. M. Ayabe, M. Kuba, and C. M. Jensen, Hydrogen bonding in sodium alanate: A muon spin rotation study, *Phys. Rev. Lett.* **100**, 026401 (2008).
- [23] J. Sugiyama, Y. Ikedo, M. Månsson, J. H. Brewer, S. L. Stubbs, E. J. Ansaldo, K. H. Chow, J. S. Lord, H. Ohta, C. Michioka, and K. Yoshimura, Magnetic and superconducting nature of $\text{Na}_{0.35}\text{CoO}_2 \cdot y\text{H}_2\text{O}$ and $\text{Na}_{0.35}\text{CoO}_2 \cdot y\text{D}_2\text{O}$ investigated by muon-spin spectroscopy, *Phys. Rev. B* **82**, 214505 (2010).
- [24] K. E. Newman, J. C. Brodovitch, and P. W. Percival, Observation of two distinct diamagnetic muon signals in the liquid phase using selective paramagnetic relaxation, *Chem. Phys. Lett.* **113**, 347 (1985).
- [25] B. D. Patterson, Muonium states in semiconductors, *Rev. Mod. Phys.* **60**, 69 (1988).
- [26] P. W. Percival, J. C. Brodovitch, K. E. Newman, and D. P. Spencer, Evidence for anisotropic diffusion of μ in ice and implications for H, *Chem. Phys. Lett.* **93**, 366 (1982).
- [27] A. Le Yaouanc and P. D. De Reotier, *Muon Spin Rotation, Relaxation, and Resonance: Applications to Condensed Matter* (OUP, Oxford, 2011), p. 147.
- [28] J. M. Wilkinson and S. J. Blundell, Information and decoherence in a muon-fluorine coupled system, *Phys. Rev. Lett.* **125**, 087201 (2020).
- [29] N. Bjerrum, Structure and properties of ice, *Science* **115**, 385 (1952).
- [30] S. K. Leung, J. C. Brodovitch, P. W. Percival, D. Yu, and K. E. Newman, The reaction of muonium with hydrated electrons, *Chem. Phys.* **121**, 393 (1988).
- [31] C. Fecko, J. Eaves, J. Loparo, A. Tokmakoff, and P. Geissler, Ultrafast hydrogen-bond dynamics in the infrared spectroscopy of water, *Science* **301**, 1698 (2003).
- [32] J. Lord, Computer simulation of muon spin evolution, *Physica B: Condens. Matter* **374-375**, 472 (2006).
- [33] O. Behnke, K. Kroninger, G. Schott, and T. Schorner-Sadenius, *Data Analysis in High Energy Physics: A Practical Guide to Statistical Methods* (John Wiley & Sons, New York, 2013).
- [34] M. Shiga, M. Tachikawa, and S. Miura, *Ab initio* molecular orbital calculation considering the quantum mechanical effect of nuclei by path integral molecular dynamics, *Chem. Phys. Lett.* **332**, 396 (2000).
- [35] M. Shiga, M. Tachikawa, and S. Miura, A unified scheme for *ab initio* molecular orbital theory and path integral molecular dynamics, *J. Chem. Phys.* **115**, 9149 (2001).
- [36] G. Kresse and J. Furthmüller, Efficiency of *ab-initio* total energy calculations for metals and semiconductors us-

- ing a plane-wave basis set, *Comput. Mater. Sci.* **6**, 15 (1996).
- [37] G. Kresse and J. Furthmüller, Efficient iterative schemes for *ab initio* total-energy calculations using a plane-wave basis set, *Phys. Rev. B* **54**, 11169 (1996).
- [38] E. Roduner and I. D. Reid, Hyperfine and structural isotope effects in muonated cyclohexadienyl and cyclopentyl radicals, *Isr. J. Chem.* **29**, 3 (1989).
- [39] Y. K. Chen, D. G. Fleming, and Y. A. Wang, Theoretical calculations of hyperfine coupling constants for muoniated butyl radicals, *J. Phys. Chem. A* **115**, 2765 (2011).
- [40] K. Yamada, Y. Kawashima, and M. Tachikawa, Accurate prediction of hyperfine coupling constants in muoniated and hydrogenated ethyl radicals: *Ab initio* path integral simulation study with density functional theory method, *J. Chem. Theory Comput.* **10**, 2005 (2014).